Published in final edited form as:
Nat Immunol. 2010 April ; 11(4): 303–312. doi:10.1038/ni.1853.

CD169+ MACROPHAGES PRESENT LIPID ANTIGENS TO MEDIATE EARLY ACTIVATION OF INVARIANT NKT CELLS IN LYMPH NODES

Patricia Barral[1], **Paolo Polzella**[2], **Andreas Bruckbauer**[1], **Nico van Rooijen**[3], **Gurdyal S. Besra**[4], **Vincenzo Cerundolo**[2,*], and **Facundo D. Batista**[1,*]

[1]Lymphocyte Interaction Laboratory, Cancer Research UK, London Research Institute, 44 Lincoln's Inn Fields, London WC2A 3PX, UK [2]Tumor Immunology Group, Weatherall Institute of Molecular Medicine, John Radcliffe Hospital, Headington, Oxford OX3 9DS, UK [3]Department of Molecular Cell Biology, Faculty of Medicine, Vrije Universiteit, VUMC, Van der Boechorststraat 7, 1081 BT Amsterdam, The Netherlands [4]School of Biosciences, University of Birmingham, Edgbaston, Birmingham B15 2TT, UK

Abstract

Invariant NKT (*i*NKT) cells are involved in host defence against microbial infections. While it is known that *i*NKT cells recognize glycolipids presented by CD1d, how and where they encounter antigen *in vivo* remains unclear. We used multi-photon microscopy to visualize the dynamics and activation of *i*NKT cells in lymph nodes. Following antigen administration, *i*NKT cells become confined in a CD1d-dependent manner in close proximity to subcapsular sinus $CD169^+$ macrophages. These macrophages retain, internalize and present lipid antigen, and are required for *i*NKT cell activation, cytokine production and expansion. Thus, $CD169^+$ macrophages can act as *bona fide* antigen presenting cells controlling early *i*NKT cell activation and favouring fast initiation of immune responses.

INTRODUCTION

Invariant NKT (*i*NKT) cells are a specialized subset of classical αβ T lymphocytes implicated in a wide range of immune responses including anti-viral, anti-bacterial, inflammatory and autoimmune reactions1. *i*NKT cells are characterised by the expression of a restricted αβ T cell receptor (TCR) repertoire comprised of the canonical $V_\alpha14$-$J_\alpha18$ chain in association with the $V_\beta2$, $V_\beta7$ or $V_\beta8$ chains in mice (equivalent to $V_\alpha24$-$J_\alpha18$ and $V_\beta11$ in humans)2. Through these TCRs *i*NKT cells specifically recognize lipid antigens presented by CD1d, a MHC class I-like molecule expressed by professional antigen presenting cells (APCs), including dendritic cells (DCs), macrophages and B cells3. Several lipid antigens capable of directly activating *i*NKT cells have been identified including glycolipids from LPS-negative bacteria such as *Sphingomonas, Erlichia* and *Borrelia4-6*.

[*]**Corresponding author:** Facundo D. Batista, facundo.batista@cancer.org.uk, Tel: +44 (0) 20 7269 2059, Fax: +44 (0) 20 7269 3479; Vincenzo Cerundolo, vincenzo.cerundolo@imm.ox.ac.uk, Tel: +44 1865 222412, Fax: +44 1865 222502.

AUTHORS CONTRIBUTIONS

P.B. and F.D.B. design and conceptualized the research in frequent consultation with V.C. and P.P; P.B. performed all the experiments; P.P. made some initial observations that lead to the development of the study and constantly provide reagents; A.B. assisted with the multi-photon microscopy; N.vR. provided clodronate liposomes; G.B. provided Gal(α1→2)α-GalCer; P.B and F.D.B. prepared the manuscript in consultation with V.C. and P.P.

The authors declare that they have no competing financial interests.

Europe PMC Funders Author Manuscripts

Furthermore, it has been suggested that in response to TLR stimulation of professional APCs, a combination of enhanced IL-12 secretion and up-regulation of endogenous lipid(s) may also activate *i*NKT cells in a CD1d dependent6-9 or independent manner10. Activated *i*NKT cells very rapidly secrete large quantities of cytokines, such as IFN-γ and IL-4, and induce downstream activation of a variety of other cell types, including DCs, NK cells, B cells and classical T cells. Thus *i*NKT cells can play a pivotal position in coordinating both innate and adaptive immune responses1,2.

*i*NKT cells occupy a similar tissue distribution to classical αβ T cells2 though the relative proportion of *i*NKT cells varies according to the particular location. For example, *i*NKT cells comprise around 30%, 2-3% and up to 0.5% of the total αβ T cell population in the liver, spleen and lymph nodes (LNs) respectively. Under physiological conditions of clonal abundance, *i*NKT cells exceed the number of antigen-specific αβ T cells by around 500 to 5000-fold in the LN (~1 in 10^5-10^6 T cells11). Thus, though the relative number of *i*NKT cells in secondary lymphoid tissues may appear small on first examination, it is likely that they make an important contribution in the regulation of immune responses in these sites. However, very few studies up to date have attempted to investigate the role of *i*NKT cells in the LNs12,13.

In spite of the key role of *i*NKT cells in host defence against microbial infections14, the mechanism by which these cells encounter antigen and become activated *in vivo* has not been fully investigated. As CD1d is expressed on a wide variety of cell types15, many cells could be potentially involved in mediating antigen presentation and subsequent activation of *i*NKT cells *in vivo*. Several studies have suggested that DCs and Kupffer cells play an important role in presenting glycolipids to *i*NKT cells in spleen and liver16,17. In fact, administration of DCs pulsed *in vitro* with bacteria such as *Sphingomonas* and *Borrelia* or different glycolipids can stimulate activation of *i*NKT cells *in vivo*4-6,16. Two studies have analyzed the behaviour of a population of $CXCR6^+$ cells (mainly comprised of NKT cells) in the liver by confocal microscopy18, 19. These studies demonstrate that $CXCR6^+$ cells become arrested within hepatic sinusoids following administration of antigenic lipids. However, the events underlying *i*NKT cell activation, including the cells involved in antigen internalization and presentation, have not been fully investigated in living lymphoid organs.

Much of the current understanding of the mechanisms of antigen presentation and lymphocyte activation in secondary lymphoid organs has been uncovered through innovative intravital imaging in the LN20. Following administration, a first wave of antigen is rapidly delivered to draining LNs through afferent lymphatic vessels and moved around the subcapsular sinus (SCS). Large antigens such as viruses, pathogens and immune complexes, are restricted from gaining access to the LN interior as they are retained by cells lining the SCS and presented to antigen-specific B and T cells directly in the LN periphery21-25. Several hours after the initial administration, a second wave of antigen arrives to the LN in association with migratory peripheral DCs allowing presentation to cognate T lymphocytes deep in the LN cortex26. It is likely that during an immune response these two waves of presentation collaborate to maximise the probability of lymphocytes encountering their cognate antigen; however the contribution (if any) that either could make to *i*NKT cell activation in the LN is not fully understood.

Here we investigate the early events that control the activation of *i*NKT cells in response to specific antigens. We have used multi-photon microscopy to visualize the dynamic behaviour of *i*NKT cells in intact LNs. We observed that *i*NKT cells are mainly located in the paracortical region, similar to classical $CD4^+$ T cells, while they search the LN for specific antigen. Within hours of administration lipid antigen retained at the SCS region stimulates the arrest of *i*NKT cells at this site. Furthermore we identified that $CD169^+$

macrophages in the SCS mediate long-lasting interactions with *i*NKT cells in a CD1d-dependent manner, which results in very fast *i*NKT cell activation and cytokine secretion. Thus, we have identified a further role for SCS macrophages in presenting lipid antigen to mediate rapid activation of *i*NKT cells in the LN, likely to be important during the early stages of immune responses.

RESULTS

Distribution and dynamics of *i*NKT cells in the LNs

We wanted to investigate the distribution and dynamics of *i*NKT cells in the LNs. In view of the relatively small number **(**Fig. 1a and 1b), heterogeneity12,27,28 and the lack of reagents for reliable unambiguous identification of *i*NKT cells using immunohistochemistry *in situ*29 we used adoptive transfer and multi-photon microscopy to visualize *i*NKT cells in the LNs. To overcome the limitations that might be associated with the isolation of heterogeneous populations, we used two complementary flow cytometry sorting strategies that allowed us to obtain highly pure *i*NKT cells. We define these two strategies as: *i*NKT-S1, *i*NKT cells sorted from LNs as α-galactosylceramide (α-GalCer)-loaded CD1d-tetramer (CD1d-tet)$^+$TCRβ$^+$B220$^-$ cells (>97% purity; **Supplementary Fig. 1a** and **1b**); and *i*NKT-S2, *i*NKT cells sorted from spleen and liver as TCRβ$^+$NK1.1$^+$B220$^-$ cells (> 95% CD1d-tet$^+$ cells; Fig. 1c and Supplementary Fig. 2a). While larger numbers of *i*NKT cells were obtained from spleen and liver, *i*NKT cells sorted from LNs more closely represented the relative proportions of NK1.1$^+$/NK1.1$^-$ *i*NKT cells found in LNs of WT animals (Supplementary Fig. 1**)**. The resulting *i*NKT cells sorted by these two approaches were transferred independently into C57BL/6 recipient mice. Regardless of the tissue of origin or the purification strategy, transferred *i*NKT cells home to LNs where they represent around 0.05 - 0.1% of total TCRβ$^+$ T cells (Fig. 1d, Supplementary Fig. 1c and Supplementary Fig. 2b). Thus both strategies allow analysis of *i*NKT cell distribution in conditions resembling those of clonal abundance in resting LNs where endogenous *i*NKT cells represent around 0.3% of total T cells.

To visualize *i*NKT cell distribution in the LN, *i*NKT-S1 and *i*NKT-S2 cells were CFSE labelled and independently transferred into C57BL/6 recipient mice, along with CMAC-labelled B cells and SNARF-1-labelled CD4$^+$ T cells to define follicular and paracortical regions of the LNs respectively. Sixteen hours after transfer, mice were sacrificed and LNs removed, fixed and imaged intact using multi-photon microscopy. We acquired adjacent 5 μm sections through the LN and assembled them in three dimensions to allow visualization of *i*NKT cells up to a depth greater than 400 μm below the surface of the node (Fig. 1e and 1f; **Supplementary Fig. 1d** and **1e**). Independently of the tissue of origin or the purification strategy, *i*NKT cells were preferentially located in the paracortex alongside CD4$^+$ T cells. While on analysis of Z-projected images *i*NKT cells were occasionally found in the B cell follicles, careful examination of three-dimensional reconstructions of the LNs revealed that these *i*NKT cells were located around the periphery of follicles and were essentially excluded from the B cell areas. Around 10% of *i*NKT cells were detected in interfollicular regions or in close proximity to the SCS (Fig. 1e and 1f; **Supplementary Fig. 1d** and **1e**).

To characterise the dynamics of *i*NKT cells in living LNs, we used multi-photon microscopy to image intact LNs from mice having undergone adoptive transfer of *i*NKT cells purified using both regimes described above. We observed that *i*NKT cells traverse the LN with an average speed of 11.0 ± 3.1 and 10.0 ± 3.2 μm/min, for *i*NKT-S1 and *i*NKT-S2 respectively (Fig. 1g and Supplementary Movies 1 and 2). *i*NKT cells average speed was similar to that of co-transferred CD4$^+$ T cells and was around two-fold greater than co-transferred B cells (measured at 10.1 ± 4.0 μm/min and 5.4 ± 2.4 μm/min respectively), in agreement with previous observations20,30. A closer inspection showed that the distribution of

instantaneous speeds for individual *i*NKT and $CD4^+$ T cells was comparable, with maxima around 30 μm/min (Fig. 1h). To gain insight into the nature of the movements of *i*NKT cells in the LN, we used the arrest coefficient to represent the proportion of the time during a given track in which a cell is stopped (Fig. 1i). In addition, the confinement index denoted whether cells are restricted to a particular area during the imaging period (Fig. 1j). This analysis revealed that *i*NKT cells behave in a similar manner to $CD4^+$ T cells, showing comparable arrest coefficient and confinement index values (Fig. 1i and 1j). Furthermore, the mean absolute displacement increased proportionally with the square root of time (Fig. 1k) indicating that both *i*NKT and $CD4^+$ T cells move in a random walk mode20,30. Based on this representation we calculated a motility coefficient of 70.3 ± 17.1 and 65.9 ± 4.6 μm^2/min for *i*NKT-S1 and *i*NKT-S2 cells respectively, and 73.8 ± 14.4 μm^2/min for $CD4^+$ T cells, indicating that these cells are able to scan similar volumes of the LN in a given time.

Importantly, *i*NKT cells purified through our two different strategies display comparable distributions and dynamics in the LN, independent of their tissues of origin or purification method. Therefore we conclude that *i*NKT cells are predominantly located in the paracortical region and patrol resting LNs with a random walk exhibiting similar dynamic characteristic to classical $CD4^+$ T cells.

Early activation of LN *i*NKT cells

Next we examined whether *i*NKT cells are activated by lipid antigens drained into LNs. To mimic conditions occurring during infection with bacteria encoding *i*NKT cell agonists4-6,14, we injected silica particles of 200 nm in diameter31 coated with α-GalCer (200 ng α-GalCer per 1μl particles, ~10^9 particles/μl). Particles coated with non stimulatory lipids were used as controls in all experiments31. WT C57BL/6 mice were injected with particulate α-GalCer and, by 3 days after injection, LNs were found to be enlarged, exhibiting an increase in cell number around 3 times compared with LNs from animals injected with control particles (Fig. 2a and 2b). This enlargement was dependent on the presence of *i*NKT cells as it was not detected in $J_\alpha 18$ KO animals (lacking NKT cells) injected with α-GalCer particles (Fig. 2b). In spite of the increased cellularity, the relative proportion of different cell types (including B, T, NK and DCs) was unaffected, except for *i*NKT cells that were highly enriched in the LNs of animals injected with particulate α-GalCer with respect to control animals (Fig. 2c-f). Accordingly, the frequency of *i*NKT cells in draining LNs, but not in non-draining nodes, was increased up to 10-fold compared with total $TCR\beta^+$ cells (Fig. 2d-f). As such, intraperitoneal (i.p.) injection of particulate antigen increased the frequency of *i*NKT cells in the mediastinal LN (Fig. 2e), consistent with the notion that mediastinal LNs drain the peritoneal cavity32,33, while subcutaneous (s.c.) footpad injection enlarged the population of *i*NKT cells in the draining popliteal LN (Fig. 2f). We detected no change in the frequency of *i*NKT cells in draining LNs following injection of control particles coated with non-stimulatory lipids (Fig. 2d). Moreover, we observed CFSE dilution of adoptively transferred *i*NKT cells 2 days after injection of particulate lipid antigen, indicating that the increased frequency of *i*NKT cells in draining LNs was due, at least in part, to antigen-induced proliferation (Fig. 2g).

When we analyzed the activation of endogenous *i*NKT cells within the first hours after antigen administration we detected that, as soon as 6 h after injection, *i*NKT cells in draining LNs up-regulated the expression of CD25 (Fig. 2h-2j) and CD69 (Fig. 2k), indicating that antigen recognition takes place in the nodes in the very early hours after administration. Moreover, both $NK1.1^+$ and $NK1.1^-$ *i*NKT cell populations in the LNs showed identical CD25 and CD69 up-regulation after injection of particulate lipid antigen (Fig. 2l). In agreement with the ability of *i*NKT cells to rapidly secrete large amounts of cytokines after activation27, we observed production of IFN-γ by LN *i*NKT cells at 12 h after antigen

injection, which was detected by *ex vivo* intracellular staining of LN single cell suspensions without addition of brefeldin A (Fig. 2m).

Thus, *i*NKT cells are rapidly activated in the LNs in response to antigen administration, indicating that they can play a role in the early initiation of immune responses in draining nodes.

*i*NKT cell dynamics in response to specific antigen

Previous investigations have revealed that the dynamics of B and T cells in LNs are altered following administration of cognate antigen20. Accordingly, we used multi-photon microscopy to examine the dynamics of *i*NKT cells adoptively transferred into C57BL/6 WT mice in the LN at various times after administration of particulate lipid antigen.

We observed that *i*NKT cells exhibit a decrease in average speed as soon as 2 h after injection of particulate lipid antigen (6.5 ± 3.4 μm/min for *i*NKT-S2 cells) which became more apparent by 16 h after injection (3.8 ± 2.4 μm/min and 2.9 ± 1.8 μm/min for *i*NKT-S2 and *i*NKT-S1 cells respectively; Fig. 3a, Supplementary Fig. 3a and Supplementary Movies 3 and 4). This decrease in speed was accompanied by an increase in long-lasting arrests, that is reflected both in the altered distribution of instantaneous speeds (Fig. 3b and Supplementary Fig. 3b) and in the increased arrest coefficient (Fig. 3c and Supplementary Fig. 3c). In addition we observed that *i*NKT cells become more confined following antigen administration, as evidenced by the constriction of the migratory trajectories (Fig. 3d and Supplementary Fig. 3e) and increase in confinement index (Fig. 3e and Supplementary Fig. 3d). Furthermore, the motility coefficient of *i*NKT cells is reduced around 10-fold to 5.0 ± 2.8 μm^2/min and 3.8 ± 3.3 μm^2/min for *i*NKT-S2 and *i*NKT-S1 cells respectively in response to particulate lipid antigen (Fig. 3f and Supplementary Fig. 3f). The speed and confinement of $CD4^+$ T cells were not affected following injection of particles coated with lipid antigen (Fig. 3a-3f and Supplementary Fig. 3). *i*NKT cells purified using our two different strategies showed identical dynamic behaviour in response to the administration of specific antigen.

To ascertain if the observed arrest of *i*NKT cells is dependent on CD1d-mediated antigen presentation, we used CD1d-deficient mice as recipients for adoptive transfer of *i*NKT-S2 and $CD4^+$ T cells. 16 h after administration of particulate lipid antigen, *i*NKT cells behaved in a similar manner to $CD4^+$ T cells and did not exhibit a decrease in average speed (Fig. 3g and Supplementary Movie 5). In addition, the migratory trajectories and confinement index of *i*NKT cells transferred into CD1d-deficient mice were not altered following administration of antigen (Fig. 3h and 3i). Thus, in the absence of CD1d-mediated presentation, the behaviour of *i*NKT cells in response to specific antigen administration is indistinguishable from $CD4^+$ T cells.

Taken together, these findings demonstrate that LN *i*NKT cells become confined as a result of CD1d-mediated antigen presentation within hours of administration of particulate lipid antigen.

*i*NKT cells arrest on $CD169^+$ SCS macrophages

Given that *i*NKT cells in draining LNs are activated in response to specific lipid antigen in a CD1d-dependent manner, we investigated both the site and the APCs involved in antigen presentation to *i*NKT cells. To achieve this we used fluorescent-labelled particulate lipids and tracked their distribution in the LNs through a combination of flow cytometry and confocal microscopy alongside multi-photon microscopy. Within minutes of injection, we detected particulate lipid antigen primarily within the SCS and medullary regions of the draining LNs (Supplementary Fig. 4a-4e). When we visualized the behaviour of *i*NKT-S2

cells in the LN after antigen arrival by multi-photon microscopy we observed that, as soon as 2 h after injection, adoptively transferred *i*NKT cells move towards the SCS and are confined in the vicinity of antigen-rich areas (Fig. 4a, Supplementary Fig. 5a and Supplementary Movie 6). Further, 16 h after antigen administration, these *i*NKT cells were predominantly observed in the LN periphery and, in agreement with our earlier data, exhibited long-lasting arrests (Fig. 4b, Supplementary Fig. 5b and Supplementary Movie 7). *i*NKT-S1 cells were also found in close proximity to the SCS region 16 h after injection of particulate lipid antigen (Supplementary Fig. 5c and Supplementary Movie 8).

$CD169^+$ macrophages can mediate retention of antigen at the SCS region of LNs21,23-25,34,35. In line with this, 2 h after administration we observed particulate lipid antigen arriving to the LNs and localizing within $CD169^+$ macrophages and in association with $LyVE\text{-}1^+$ lymphatic vessels (Fig. 4c and Supplementary Fig. 4f). Accordingly, particles were detected with more than 50% of $CD169^+$-$CD11b^+$ cells in the draining LNs by flow cytometry within 4 h of antigen administration (Fig. 4d). No antigen retention by $CD11c^{hi}$ conventional DCs was observed at this time point (Fig. 4c and 4d). To further characterise the behaviour of LN *i*NKT cells after antigen arrival, we visualized *i*NKT-S2 cells in recipient animals injected with fluorescently labelled anti-mouse CD169 antibody34 alongside with labelled particulate α-GalCer or control lipids (Fig. 4e). We fixed the LNs of recipient animals, imaged them by multi-photon microscopy and analyzed the location of *i*NKT cells relative to SCS $CD169^+$ macrophages. $CD169^+$ cells formed a layer in the SCS of the LNs retaining particulate lipids (Fig. 4e). Within 6 h of antigen administration, we observed that *i*NKT cells are retained in the vicinity of the SCS and approximately 55% (40 out of 75 *i*NKT cells) establish direct contact (< 5μm apart) with $CD169^+$ macrophages (Fig. 4e and 4f). In contrast, following administration of particles containing non-stimulatory lipids *i*NKT cells were predominantly located in deeper regions of the LN with few (18%, 10 out of 54 *i*NKT cells) making contact with SCS macrophages (Fig. 4e and 4f). Furthermore imaging of living LNs revealed *i*NKT cells stopping in the SCS region and establishing long-lasting interactions with particle-containing macrophages by 6 h after antigen injection. A large proportion of *i*NKT cell-macrophage contacts (81%, 59 out of 73) lasted for the duration of the 20 min imaging period and dissociation of these conjugates was rarely observed (19%, 14 out of 73) (Fig. 4g and Supplementary Movies 9 and 10).

Thus, *i*NKT cells make specific and long-lasting contacts with antigen-loaded $CD169^+$ macrophages within few hours of antigen arriving at the draining LN.

*i*NKT cell activation by LN macrophages

To establish if macrophages are capable of mediating *i*NKT cell activation in the LNs, we depleted resident macrophages by treatment with clodronate liposomes (CLL). In agreement with previous reports23 we observed that CCL preferentially depleted macrophages only in draining LNs leaving non draining LNs intact (data not shown). Though CLL treatment induced an increase in total cell numbers in draining LNs, it did not alter the relative proportions of B, T, DC and *i*NKT cells (Fig. 5a and 5b; Supplementary Fig. 6a) or the gross morphological structure of the LN (Supplementary Fig. 6c). In addition, macrophage depletion did not affect the basal state of *i*NKT cells as the expression of CD25 remained unchanged after CLL treatment (Supplementary Fig. 6b).

To analyze the role of macrophages in *i*NKT cell activation we injected macrophage-depleted and control animals with particulate lipids. In the absence of macrophages, particulate lipids were predominantly detected deep in the B cell follicles and in medullary regions (Supplementary Fig. 6d). By 12 h after injection of particulate lipid antigen we observed that CD25 up-regulation by *i*NKT cells was decreased around two-fold in draining LNs of CCL treated with respect to untreated animals (Fig. 5c). Furthermore, macrophage

depletion prevented the expansion of *i*NKT cells 3 days after administration of antigen as reflected in the percentage and number of *i*NKT cells found in draining LNs (Fig. 5d-5f). Therefore, selective macrophage depletion in the LNs leads to inefficient *i*NKT cell activation and prevents the expansion of the *i*NKT cell population.

CD169$^+$ macrophages mediate CD1d-dependent antigen presentation

Next, we investigated the possibility that CD169$^+$ macrophages participate directly in the presentation of antigenic lipids to *i*NKT cells. In line with this, we observed that CD169$^+$ macrophages expressed cell surface CD1d by flow cytometry (Fig. 6a). Subsequently, CD11b$^+$ cells were enriched from LN single cell suspensions by magnetic selection and CD169$^+$-CD11b$^+$ macrophages were highly purified by flow cytometry sorting (Fig. 6b). After pre-incubation for 2 h with particulate lipids, CD169$^+$ macrophages were co-cultured with mouse *i*NKT hybridoma DN32.D3 cells. α-GalCer was efficiently presented by CD169$^+$ cells, as defined by IL-2 production by DN32.D3 cells (Fig. 6c**)**. To ascertain if *i*NKT activation is dependent on antigen internalization, we used particles containing Gal(α1→2)α-GalCer, an α-GalCer analogue that requires intracellular processing prior to recognition by *i*NKT cells36. Co-culture of DN32.D3 cells with macrophages pre-incubated with Gal(α1→2)α-GalCer particles induced secretion of IL-2 (Fig. 6d), indicating that *i*NKT cell activation is indeed dependent on antigen internalization by macrophages. Moreover we observed that CD169$^+$ macrophages were able to present antigen to a similar extent as CD11c^{hi} DCs purified from mice LNs (Fig. 6e). In contrast, LN B cells were not able induce IL-2 secretion in co-cultured DN32.D3 *i*NKT cells (Fig. 6e), in line with their low phagocytic capacity in absence of specific BCR-mediated uptake31.

CD169$^+$ macrophages can be distinguished as SCS or medullary macrophages on the basis of F4/80 expression35. Therefore, we sought to determine if macrophages from the SCS were capable of lipid antigen presentation by purifying them as CD169$^+$CD11b$^+$CD11c^{int} F4/80$^-$ cells from mice LNs (Fig. 6f and Supplementary Fig 7). Indeed, we observed that SCS macrophages were able to present lipid antigens to co-cultured DN32.D3 *i*NKT cells as evidenced by IL-2 secretion (Fig. 6g).

As purified macrophages are able to present lipid antigen to *i*NKT cells *in vitro*, we assessed the ability of CD169$^+$ cells to retain and present particulate α-GalCer *in vivo*. To do this, we injected animals with particles coated with α-GalCer or control lipids and 2 h later CD169$^+$ cells were purified from draining LNs and incubated *in vitro* with DN32.D3 *i*NKT cells. Only CD169$^+$ macrophages from animals injected with particulate α-GalCer stimulated IL-2 secretion from DN32.D3 cells (Fig. 6h). In a similar manner, CD169$^+$ cells purified from draining nodes of WT mice injected with Gal(α1→2)α-GalCer coated particles, gave rise to IL-2 secretion from co-cultured DN32.D3 cells (Fig. 6i). CD169$^+$ macrophages purified from draining LNs of animals injected with control particles were unable to induce IL-2 secretion by DN32.D3 cells (Fig. 6h and 6i). Furthermore, while LN DCs were capable of lipid antigen presentation *in vitro*, neither CD11c^{hi} DCs nor B cells purified from draining LNs 2 h after injection of particulate α-GalCer were able to stimulate IL-2 secretion from co-cultured DN32.D3 cells (Fig 6j).

Finally, to establish if CD169$^+$ macrophages can present antigen to primary LN-*i*NKT cells, we performed presentation assays with CD169$^+$ cells and CFSE-labelled primary *i*NKT-S1 cells purified from mouse LNs (Fig. 6k and 6l). CD169$^+$ macrophages pulsed with particulate α-GalCer were able to induce IFN-γ secretion (Fig. 6k) and proliferation of primary LN-*i*NKT cells as evidenced by CFSE dilution (Fig. 6l). In the absence of macrophages or when *i*NKT cells were co-cultured with CD169$^+$ cells pulsed with control lipids, no proliferation or IFN-γ secretion was detected for primary *i*NKT cells (Fig. 6l).

Europe PMC Funders Author Manuscripts

Thus, CD169$^+$ macrophages internalize antigenic lipids both *in vitro* and *in vivo*, and can present them in association with CD1d to efficiently activate *i*NKT cells.

Bacterial glycolipids stimulate macrophage-dependent *i*NKT cell activation

To verify our findings with an *i*NKT cell agonist derived from bacterial glycolipids, silica particles were coated with liposomes containing α-linked galacturonic glycosphingolipid (GSL-1′) expressed by *Sphingomonas yanoikuyae,* which can activate *i*NKT cells5,37. We observed that particulate GSL-1′ induced a 1.6-fold increase in the total number of cells in the LN compared with LNs from animals injected with control particles (Fig. 7a). This enlargement was dependent on the presence of *i*NKT cells as it was not detected in $J_\alpha 18$ KO animals (lacking NKT cells) injected with GSL-1′-coated particles (Fig. 7a). While the relative proportion of DCs, B and T cells remained the same, LN *i*NKT cells were enriched up to 3-fold upon injection of particulate GSL-1′ (Fig. 7b). In addition we observed that *i*NKT cells in draining LNs up-regulate CD25 and CD69, and produce IFN-γ within few hours of particulate GSL-1′ administration (Fig. 7c-7f). To test whether *i*NKT cell responses to *Sphingomonas* glycolipids were also dependent on LN resident macrophages, we specifically depleted LN macrophages by CLL treatment. After administration of particulate GSL-1′, *i*NKT cells were not efficiently activated in draining LNs of CLL-treated animals, showing up to a three-fold decrease in CD25 up-regulation compared to *i*NKT cells in the LNs from untreated animals (Fig. 7g). Finally, we adoptively transferred labelled *i*NKT-S1 cells and CD4$^+$ T cells into WT recipients to visualize the dynamics of *i*NKT cells in response to particulate GSL-1′ (Supplementary Movie 11). In contrast to CD4$^+$ T cells, *i*NKT cells exhibited a significant decrease in speed to 7.3 + 3.6 μm/min 16 h after particulate GSL-1′ administration (Fig. 7h). This was accompanied by an increase in long-lasting arrests reflected by the altered distribution of instantaneous speeds (Fig. 7i), the increased arrest coefficient (Fig. 7j) and the decreased motility coefficient (31.2 ± 9.9 μm^2/min; Fig. 7k).

Thus, similar to α-GalCer, bacterial glycolipids can mediate the early activation of *i*NKT cells in draining LNs in a manner dependent on the presence of macrophages.

DISCUSSION

This study provides new insight into the early events of *i*NKT cell activation in the LNs *in vivo*. We have imaged *i*NKT cells in living lymphoid tissues showing that they patrol the LN paracortex in resting conditions. Within minutes after administration, lipid antigens arrive to the SCS of the LNs where they are retained and presented to *i*NKT cells. Cognate antigen recognition induces *i*NKT cell arrest and leads to cytokine production and expansion of the *i*NKT cell population. Finally, we demonstrate that CD169$^+$ macrophages play a critical role in *i*NKT cell activation as they retain, internalize and present lipids to *i*NKT cells acting as *bona fide* APCs in the LNs.

Over the past decade much effort has been expended in the search for lipid antigens that bind CD1d molecules and activate *i*NKT cells2,14 however, very little is known about how and where *i*NKT cells encounter antigen *in vivo*. In fact, to date very few studies have achieved the visualization of *i*NKT cells *in situ*, probably due to the lack of reliable reagents that allow their identification. In this line, we and others have unsuccessfully tried to visualize *i*NKT cells by immunohistochemitry using CD1d-tet29. On the other hand, the use of less stringent markers (like NK1.1) results in the inclusion of other cell populations making difficult the unequivocal identification of *i*NKT cells. To circumvent these issues we used two complementary strategies to purify *i*NKT cells prior to their labelling, adoptive transfer and visualization by multi-photon microscopy. Since we were concerned that the purification of *i*NKT cells with CD1d-tet could occasionally induce their partial

activation29, in a first approach we purified *i*NKT cells from spleen and liver as TCRβ$^+$NK1.1$^+$ cells. However, as LN *i*NKT cells are represented by both NK1.1$^+$ and NK1.1$^-$ cells28 we verified our results by purifying *i*NKT cells from the LNs as TCRβ$^+$CD1d-tet$^+$ cells. *i*NKT cells purified by both strategies were detected in the LNs of recipient animals in similar numbers and they showed identical location and dynamic behaviours, independent of their tissue of origin or purification method. In spite of the fact that *i*NKT cell number is lower in the LNs compared with the spleen or liver population, in normal conditions of clonal abundance the number of *i*NKT cells in the LNs is between 500-5000 times higher than that for any antigen-specific T cell population11. Remarkably, the number of transferred *i*NKT cells observed in the LNs was in the same order as that of endogenous *i*NKT cells, allowing us to analyze *i*NKT cell behaviour under conditions of typical clonal abundance. As such, our adoptive transfer strategy avoided the abnormally high numbers of antigen specific cells frequently associated with this kind of experiments38. Using multi-photon microscopy imaging of living LNs, we observed that *i*NKT cells in resting conditions were predominantly located in the paracortical region where they move in random walks with average speed of around 10 μm/min. Accordingly, *i*NKT cells exhibit similar kinetic behaviour as observed for classical CD4$^+$ T cells as they scan the LN in search for specific antigen20, 30.

Although α-GalCer is derived from a marine sponge it has proven to be a very valuable tool for dissecting the pivotal role of *i*NKT cells in autoimmunity, cancer and host defence2. Indeed, the wide availability of this glycolipid allowed us to understand the uptake and presentation of lipid antigens in the LNs by CD169$^+$ macrophages that will lead to subsequent *i*NKT cell activation. Our dynamic imaging approach, in concert with our flow cytometry data, demonstrates that *i*NKT cell activation occurs within a few hours of antigen arrival at the draining LN. Furthermore, we validated these results showing that *Sphingomonas* glycolipids can rapidly activate LN *i*NKT cells inducing IFN-γ secretion, LN enlargement and altering the dynamic behaviour of *i*NKT cells in the LNs. In line with the fact that GSL-1′ is a weaker *i*NKT cell agonist compared with α-GalCer5, its effect on LN enlargement and *i*NKT cell dynamics was less marked than that observed for α-GalCer. However, GSL-1′ was efficient in inducing activation of LN *i*NKT cells as measured by CD25 and CD69 up-regulation and IFN-γ secretion. In agreement with these results, the work from Lee *et al*. (in the current issue) shows how liver *i*NKT cells are activated in response to the administration of *Borrelia burdorgferi* as reflected by the alteration in their dynamic behaviour. Therefore, our results point to a pivotal role of *i*NKT cells in the initiation of immune responses in the LNs against a variety of infectious agents.

Traditionally, *i*NKT cell activation has been studied using soluble lipids or lipid-pulsed DCs. However, during the course of an infection, antigenic lipids would be more likely present in the capsule of different pathogens like *Sphingomonas, Borrelia* or *Erlichia*4-6. On arrival to the LN, particulate antigens are retained in the SCS region where they can be directly recognized by specific lymphocytes21-25,35. In agreement with this, we observed that particulate lipids localised within the SCS very rapidly following administration. Subsequently *i*NKT cells arrest in the SCS region of the LNs within few hours after antigen administration. In line with this, naïve and memory CD8$^+$ T cells relocate close to the SCS region within few hours after antigen arrival allowing T cell activation in the LN periphery22,25. Although the low numbers of *i*NKT cells in the LNs prevent examination of the kinetic of relocation of *i*NKT cells to the LN periphery, it is conceivable that they will follow a similar behaviour to that described for classical αβ T cells. On the other hand, lipid antigens could also be presented to *i*NKT cells in the LN cortex by DCs immigrating from peripheral tissues and, in fact, skin DCs are able to present antigen to *i*NKT cells after subcutaneous injection of soluble αGalCer13. However, DC migration to draining LNs takes place several hours after antigen administration and is unlikely to play a significant

role in initiating very early immune responses26,33. Nevertheless, it is conceivable that both mechanisms of antigen presentation mediated by resident and migratory APCs collaborate to activate *i*NKT cells in different LN locations at various stages during the immune response.

CD169$^+$ macrophages can be classified as SCS or medullary based on F4/80 expression and they exhibit different endocytic and degradative capabilities that might influence their function as APCs35. Several studies have identified a role for CD169$^+$ macrophages in the SCS in presenting native antigen to follicular B cells23, 24,35 and, indeed SCS cells seem to have a higher ability to retain antigen on their surface than medullary macrophages35. However, the ability of SCS macrophages to present processed antigen to T cells is still to be established23-25,35. Our data provide formal proof that SCS CD169$^+$ macrophages can act as *bona fide* APCs, internalizing and presenting lipid antigen to *i*NKT cells, although we do not exclude that medullary macrophages might also play a role in antigen presentation. Accordingly, depletion of LN macrophages by treating with clodronate liposomes severely impairs *i*NKT cell activation and avoids further proliferation. Although the mechanism governing the decision for antigen retention or internalization by SCS macrophages has not been characterized, this may depend on the cell surface receptors responsible for antigen binding. Indeed, in DCs, antigen binding through FcγRIIB leads to retention and/or recycling of intact antigen to the surface whereas binding through FcγRI and FcγRIII targets antigen for intracellular degradation39. Thus, DCs are capable of presenting antigen to both T and B cells40,41. Recognition of microbial lipids by *i*NKT cells in the context of an infection may require internalization of the pathogen through different sets of surface receptors and the release of the microbial glycolipids in intracellular compartments before loading in CD1d. In line with this, it has been suggested that CD169 (also known as sialoadhesin) could be involved in regulating the function of different immune cells, either by favouring cell-cell interactions or by functioning as a phagocytic receptor to clear sialylated pathogens42. However, the identification of the molecules expressed on the surface of macrophages that could play a direct role in modulating *i*NKT cell responses will require further investigation.

Activation of *i*NKT cells may have important implications for the outcome of immune responses as these cells have been described as a bridge between adaptive and innate immune responses for their capacity to make rapid responses that lead to downstream activation of many other cell types1,16,43. Indeed, mice lacking *i*NKT cells have a reduced clearance after infection with several pathogens like *Sphingomonas* or *Erlichia*5,6,14. Moreover, *i*NKT-deficient animals exhibit enhanced mortality in response to infection with influenza virus, as a result of a reduction in specific T and B cell responses and of an expansion of myeloid-derived suppressor cells44. Thus, while we have demonstrated that CD169$^+$ macrophages are able to present antigen to *i*NKT cells at the start of an immune response, it is conceivable that *i*NKT cells interact in an antigen-dependent manner with other cell types during the initiation or at later stages of an immune reaction. In this line, it is known that several hours after injection antigen-loaded DCs arrive to the LNs where they are able to interact with antigen-specific T cells26. *i*NKT cells could therefore interact with lipid-loaded DCs in the LNs which can lead to an increase in CD4$^+$ and CD8$^+$ T cell responses16,43. In addition, the role of *i*NKT cells in helping antigen specific B cell proliferation and antibody production is well-established31,45,46. Specific B cells take up antigen on its arrival to the LNs and subsequently migrate towards the border between the B cell and the T cell area where they form stable conjugates with antigen specific T cells47. Our preliminary data suggest that B cell-*i*NKT cell interactions can take place in the LNs within 1-2 days of antigen administration and result in B cell activation and proliferation (P.B. and F.D.B, unpublished data). Consequently, it is conceivable that SCS macrophages act as a platform to allow antigen presentation to *i*NKT cells at the beginning of an immune response, whereas later B cell-*i*NKT cell interactions will favour the development of

adaptive immune responses. Accordingly, this adjuvant-like feature of *i*NKT cells make them great candidates for the design of new vaccination strategies1. Further studies to target antigen to SCS macrophages facilitating fast *i*NKT cell activation might allow improved vaccination approaches.

Supplementary Material

Refer to Web version on PubMed Central for supplementary material.

Acknowledgments

This work was funded by: Cancer Research UK; EMBO YIP Award (F.D.B); Royal Society Wolfson Research Merit Award (F.D.B.); Cancer Research UK (C399/A2291 and C5255/A10339) (V.C.) and The Wellcome Trust (Programme Grant 084923 V.C., G.B. and F.D.B.). P.B. was supported by a postdoctoral fellowship from the Ministerio de Education from Spain (2007-0148) and by a Marie Curie Intra-European Fellowship within the seventh European Community Framework Programme (PIEF-GA-2008-220863). P.P. was supported by a Marie Curie Fellowship, Immunanomap (MRTN-CT-2006-035946). We thank Mitchell Kronenberg (La Jolla Institute for Allergy & Immunology) and Chi-Huey Wong (Scripps Laboratories) for providing GSL-1′.

Appendix

MATERIALS AND METHODS

Mice and injections

V_α14 transgenic, CD1d KO, J_α18 KO and CD45.1 C57BL/6 mice were bred and maintained at the animal facility of the John Radcliffe Hospital, Oxford. CD1d-KO animals were provided by L. Van Kaer (Vanderbilt University School of Medicine, Nashville, USA). C57BL/6 WT mice were purchased from Charles River. All experiments were approved by the Cancer Research UK, Animal Ethics Committee and the United Kingdom Home Office.

For depletion of macrophages mice were injected with a standard suspension clodronate-loaded liposomes48 six days before analysis. Clodronate was a gift of Roche Diagnostics GmbH.

Lipids and microsphere coating

Liposomes were prepared as described31 by using: 1,2-Dioleoyl-sn-Glycero-3-Phosphocholine (Avanti Polar Lipids), α-GalCer (Alexis Biochemical), Gal(α1→2)α-GalCer (produced as described49) and/or GSL-1′ (kindly provided by Dr. Mitchell Kronenberg; La Jolla Institute for Allergy and Immunology, La Jolla, USA). Silica microspheres (200 nm, Kisker GbR) were coated with liposomes as described31. CD1d-tet was produced50 or purchased from Proimmune Ltd.

Flow cytometry

For flow cytometry staining LN single-cell suspensions were prepared as described23 and anti-mouse CD16/32 (2.4G2, BD Biosciences) was used to block non-specific antibody binding. For staining of macrophages and DCs the following anti-mouse antibodies were used: CD11b-PE (M1/70), CD45/B220-pacific blue (RA3-6B2), CD11c-APC (HL3) from BD Biosciences; CD3-pacific blue (500-A2, Caltag); CD169-FITC (3D6.112, AbDSerotec) and CD1d-biotin (1B1) followed by streptavidin-PerCP (BD Biosciences). Alternatively cells were stained with: CD45/B220-pacific blue (RA3-6B2), TCRβ-FITC (H57-597), CD3-PerCP (145-2C11), CD69-PECy7 (H1.2F3) from BD Biosciences; CD25-PE (PC61.5), NK1.1-FITC (PK136) from eBiosciences; and Cd1d-tet-APC. Dead cells were excluded by staining with DAPI (2-(4-Amidinophenyl)-6-indolecarbamidine dihydrochloride, Sigma). For intracellular IFN-γ staining cells were stained with CD45/B220-pacific blue, TCRβ-

FITC and CD1d-tet-APC before fixation and permeabilization with Cytofix/Cytoperm (BD Biosciences) and staining with IFN-γ-PE (XMG1.2, BD Biosciences). Data were collected on a LSRII flow cytometer (Becton Dickinson) and analyzed with FlowJo (TreeStar).

Purification of LN macrophages and DCs

For purification, $CD11b^+$ cells were enriched from LN single-cell suspensions with CD11b-magnetic beads (Miltenyi Biotec) before sorting with anti-CD11b-APC (M1/70) and CD169-FITC (3D6.112,) on a FACSAria (Becton Dickinson).

For purification of SCS macrophages and DCs, B, T and $F4/80^+$ cells were depleted by incubation with anti-B220 (RA3-6B2, BD Biosciences), anti-CD3 (145-2C11, eBiosciences) and anti-F4/80 (BM8, Biolegend) biotinylated antibodies followed by streptavidin-magnetic beads (Dynabeads-Invitrogen). SCS macrophages and DCs were sorted as $CD169^+CD11b^+CD11c^{int}$ and $CD11c^{hi}CD169^-CD11b^+$ respectively by staining with CD11b-APC (M1/70), CD169-FITC (3D6.112) and CD11c-PE (HL3) antibodies.

Purification of *i*NKT, $CD4^+$ T and B cells

*i*NKT cells were purified from liver, spleen and LNs from $V_\alpha 14$ transgenic mice. Liver and spleen single-cell suspensions were prepared44 and *i*NKT cells sorted with TCRβ-PE (H57-597) and NK1.1-FITC (PK136) antibodies (eBioscience). Purified cells were stained with CD1d-tet-APC (>95% purity). LN *i*NKT cells were isolated by depletion of B cells with B220-magnetic beads (Dynabeads-Invitrogen) and sorting with TCRβ-PE (H57-597) and CD1d-tet-APC (>97% purity).

B and $CD4^+$ T cells were purified from spleen or LNs by using magnetic separation B or $CD4^+$ T cell isolation kits (Miltenyi Biotec).

Lipid presentation assays and ELISA

Purified macrophages, DCs or B cells were incubated with particulate lipids (2 h), washed 3 times and cultured 1-5 × 10^4 cells/well with 5 × 10^4 DN32.D3 (kindly provided by A. Bendelac; University of Chicago, IL) or primary LN-*i*NKT cells in 96 well U-bottom plates with 200 μl of RPMI 1640,10% FCS. For *in vivo* priming experiments, mice were injected with particulate lipids in the foot-pad and 2 h later $CD169^+$ cells were sorted from popliteal LNs and incubated with DN32.D3 cells as described above. IL-2 was measured by sandwich ELISA in the supernatant of the cultures, using anti-IL-2 (JES6-1A12) and biotinylated anti-IL-2 (JES6-5H4) antibodies (BD Biosciences). When primary *i*NKT cells were used IFN-γ was measured using anti-IFN-γ (R4-6A2) and biotinylated anti-IFN-γ (XMG1.2) antibodies (BD Biosciences).

Adoptive transfer

*i*NKT, $CD4^+$ T and B cells (3-4 × 10^6) were labelled with 2 μM CFSE, 2 μM SNARF-1 or 50 μM of CMAC (Molecular Probes) as described21 and injected in the tail vein of 4-6 weeks recipients. To investigate *i*NKT cell homing, CD45.1 mice were used as recipients and transferred *i*NKT cells detected by flow cytometry staining with CD45.2-APC (104; Biolegend), CD45/B220-pacific blue (RA3-6B2, BD Biosciences) and NK1.1-FITC (PK136, eBiosciences).

To investigate *i*NKT cell proliferation *in vivo*, single-cell suspensions from $V_\alpha 14$ mice spleens were prepared, B cells depleted with B220-magnetic beads and cells (~30% *i*NKT) labeled with CFSE and transferred into WT recipients injected afterwards with α-GalCer or control particles. LNs were removed 2 days later and transferred *i*NKT cells stained with

Europe PMC Funders Author Manuscripts

TCRβ-PE (H57-597, eBioscience), CD1d-tet-APC and CD45/B220-pacific blue (RA3-6B2, BD Biosciences).

Multi-photon microscopy

Mediastinal and popliteal LNs were prepared for multi-photon imaging as previously reported21. Image acquisition was performed through the capsule of the LN with an upright multi-photon microscope (Olympus Fluoview FV1000 MPE2 Twin system) using a water-immersion 25× 1.05 NA objective (Olympus XLPLNWMP) and a pulsed Ti:sapphire laser (Spectra Physics MaiTai HP DeepSee) tuned to 800 nm. For four-dimensional imaging stacks of 11-20 square xy planes spanning 508 μm by 508 μm with 5 μm z spacing were acquired over 20-30 min (30-40 time-points). Emission wavelengths were detected through 420–500 nm (CMAC), 515–560 nm (CFSE, green particles), and 590–650 nm (SNARF-1, red particles) band-pass filters. Sequences of image stacks were transformed into volume-rendered four-dimensional movies and analyzed with Imaris 6.3 × 64 software (Bitplane). Annotation and final movie compilation was performed with Adobe Photoshop CS3.0 and ImageJ. Tracks normalized at the same departure point were plotted with MatLab (The Mathworks Inc.). All statistical analysis was performed using Prism (GraphPad Software).

Immunofluorescence

Tissue sections (10 μm thick) were fixed in 4% paraformaldehyde and blocked with PBS, 1% BSA, 10% goat serum before incubation with rat anti-mouse CD45R/B220 (RA3-6B2, BD Biosciences), rat anti-mouse LyVE-1 (223322, R&D Systems) or hamster anti-mouse CD11c (N418, Caltag), followed by Alexa 633-conjugated goat anti-rat IgG or Alexa 647-conjugated goat anti-hamster IgG (Molecular Probes). Alternatively, sections were incubated with rat anti-mouse CD45R/B220-Alexa 647 (RA3-6B2, BD Biosciences), rat anti-mouse F4/80-Alexa 647 (CI:A3-1, Biolegend), rat anti-mouse CD45R/B220-FITC (RA3-6B2, BD Biosciences), rat anti-mouse CD169-FITC (3D6.112, AbDSerotec) or hamster anti-mouse CD3-FITC (145-2C11, BD Biosciences) followed by Alexa 488-conjugated anti-flourescein/Oregon green rabbit IgG (Molecular Probes) when FITC-labeled antibodies were used. Imaging was carried out on an Axiovert LSM 510-META (Zeiss) inverted microscope except for tiled images that were captured an assembled on a Fluoview FV1000 microscope (Olympus).

REFERENCES

1. Cerundolo V, Silk J, Masri SH, Salio M. Harnessing invariant NKT cells in vaccination strategies. Nat Rev Immunol. 2009; 9:28–38. [PubMed: 19079136]
2. Bendelac A, Savage PB, Teyton L. The biology of NKT cells. Annu Rev Immunol. 2007; 25:297–336. [PubMed: 17150027]
3. Brigl M, Brenner MB. CD1: antigen presentation and T cell function. Annu Rev Immunol. 2004; 22:817–890. [PubMed: 15032598]
4. Kinjo Y, et al. Natural killer T cells recognize diacylglycerol antigens from pathogenic bacteria. Nat Immunol. 2006; 7:978–986. [PubMed: 16921381]
5. Kinjo Y, et al. Recognition of bacterial glycosphingolipids by natural killer T cells. Nature. 2005; 434:520–525. [PubMed: 15791257]
6. Mattner J, et al. Exogenous and endogenous glycolipid antigens activate NKT cells during microbial infections. Nature. 2005; 434:525–529. [PubMed: 15791258]
7. Brigl M, Bry L, Kent SC, Gumperz JE, Brenner MB. Mechanism of CD1d-restricted natural killer T cell activation during microbial infection. Nat Immunol. 2003; 4:1230–1237. [PubMed: 14578883]
8. Paget C, et al. Activation of invariant NKT cells by toll-like receptor 9-stimulated dendritic cells requires type I interferon and charged glycosphingolipids. Immunity. 2007; 27:597–609. [PubMed: 17950005]

9. Salio M, et al. Modulation of human natural killer T cell ligands on TLR-mediated antigen-presenting cell activation. Proc Natl Acad Sci USA. 2007; 104:20490–20495. [PubMed: 18077358]
10. Tyznik AJ, et al. Cutting edge: the mechanism of invariant NKT cell responses to viral danger signals. J Immunol. 2008; 181:4452–4456. [PubMed: 18802047]
11. Moon J, et al. Naive CD4(+) T cell frequency varies for different epitopes and predicts repertoire diversity and response magnitude. Immunity. 2007; 27:203–213. [PubMed: 17707129]
12. Laloux V, Beaudoin L, Ronet C, Lehuen A. Phenotypic and functional differences between NKT cells colonizing splanchnic and peripheral lymph nodes. J Immunol. 2002; 168:3251–3258. [PubMed: 11907079]
13. Tripp C, Sparber F, Hermans I, Romani N, Stoitzner P. Glycolipids Injected into the Skin Are Presented to NKT Cells in the Draining Lymph Node Independently of Migratory Skin Dendritic Cells. The Journal of Immunology. 2009; 182:7644–7654. [PubMed: 19494288]
14. Tupin E, Kinjo Y, Kronenberg M. The unique role of natural killer T cells in the response to microorganisms. Nat Rev Microbiol. 2007; 5:405–417. [PubMed: 17487145]
15. Silk JD, Salio M, Brown J, Jones EY, Cerundolo V. Structural and functional aspects of lipid binding by CD1 molecules. Annu Rev Cell Dev Biol. 2008; 24:369–395. [PubMed: 18593354]
16. Fujii S, Shimizu K, Smith C, Bonifaz L, Steinman RM. Activation of natural killer T cells by alpha-galactosylceramide rapidly induces the full maturation of dendritic cells in vivo and thereby acts as an adjuvant for combined CD4 and CD8 T cell immunity to a coadministered protein. J Exp Med. 2003; 198:267–279. [PubMed: 12874260]
17. Schmieg J, Yang G, Franck RW, van Rooijen N, Tsuji M. Glycolipid presentation to natural killer T cells differs in an organ-dependent fashion. Proc Natl Acad Sci USA. 2005; 102:1127–1132. [PubMed: 15644449]
18. Geissmann F, et al. Intravascular immune surveillance by CXCR6+ NKT cells patrolling liver sinusoids. PLoS Biol. 2005; 3:e113. [PubMed: 15799695]
19. Velázquez P, et al. Cutting edge: activation by innate cytokines or microbial antigens can cause arrest of natural killer T cell patrolling of liver sinusoids. J Immunol. 2008; 180:2024–2028. [PubMed: 18250405]
20. Cahalan MD, Parker I. Choreography of cell motility and interaction dynamics imaged by two-photon microscopy in lymphoid organs. Annu Rev Immunol. 2008; 26:585–626. [PubMed: 18173372]
21. Carrasco YR, Batista FD. B cells acquire particulate antigen in a macrophage-rich area at the boundary between the follicle and the subcapsular sinus of the lymph node. Immunity. 2007; 27:160–171. [PubMed: 17658276]
22. Hickman HD, et al. Direct priming of antiviral CD8(+) T cells in the peripheral interfollicular region of lymph nodes. Nat Immunol. 2008
23. Junt T, et al. Subcapsular sinus macrophages in lymph nodes clear lymphborne viruses and present them to antiviral B cells. Nature. 2007; 450:110–114. [PubMed: 17934446]
24. Phan TG, Grigorova I, Okada T, Cyster JG. Subcapsular encounter and complement-dependent transport of immune complexes by lymph node B cells. Nat Immunol. 2007; 8:992–1000. [PubMed: 17660822]
25. Chtanova T, et al. Dynamics of T cell, antigen-presenting cell, and pathogen interactions during recall responses in the lymph node. Immunity. 2009; 31:342–355. [PubMed: 19699173]
26. Itano AA, et al. Distinct dendritic cell populations sequentially present antigen to CD4 T cells and stimulate different aspects of cell-mediated immunity. Immunity. 2003; 19:47–57. [PubMed: 12871638]
27. Kronenberg M. Toward an understanding of NKT cell biology: progress and paradoxes. Annu Rev Immunol. 2005; 23:877–900. [PubMed: 15771592]
28. Doisne J-M, et al. Skin and peripheral lymph node invariant NKT cells are mainly retinoic acid receptor-related orphan receptor (gamma)t+ and respond preferentially under inflammatory conditions. J Immunol. 2009; 183:2142–2149. [PubMed: 19587013]
29. Berzins SP, Smyth MJ, Godfrey DI. Working with NKT cells--pitfalls and practicalities. Curr Opin Immunol. 2005; 17:448–454. [PubMed: 15963710]

30. Miller MJ, Wei SH, Parker I, Cahalan MD. Two-photon imaging of lymphocyte motility and antigen response in intact lymph node. Science. 2002; 296:1869–1873. [PubMed: 12016203]
31. Barral P, et al. B cell receptor-mediated uptake of CD1d-restricted antigen augments antibody responses by recruiting invariant NKT cell help in vivo. Proc Natl Acad Sci USA. 2008
32. Tilney NL. Patterns of lymphatic drainage in the adult laboratory rat. J Anat. 1971; 109:369–383. [PubMed: 5153800]
33. Kool M, et al. Alum adjuvant boosts adaptive immunity by inducing uric acid and activating inflammatory dendritic cells. J Exp Med. 2008; 205:869–882. [PubMed: 18362170]
34. Chtanova T, et al. Dynamics of neutrophil migration in lymph nodes during infection. Immunity. 2008; 29:487–496. [PubMed: 18718768]
35. Phan T, Green J, Gray E, Xu Y, Cyster J. Immune complex relay by subcapsular sinus macrophages and noncognate B cells drives antibody affinity maturation. Nat Immunol. 2009; 10:786–793. [PubMed: 19503106]
36. Prigozy T, et al. Glycolipid antigen processing for presentation by CD1d molecules. Science. 2001; 291:664–667. [PubMed: 11158680]
37. Kinjo Y, et al. Natural Sphingomonas glycolipids vary greatly in their ability to activate natural killer T cells. Chem Biol. 2008; 15:654–664. [PubMed: 18635002]
38. Badovinac V, Haring J, Harty J. Initial T cell receptor transgenic cell precursor frequency dictates critical aspects of the CD8(+) T cell response to infection. Immunity. 2007; 26:827–841. [PubMed: 17555991]
39. Bergtold A, Desai D, Gavhane A, Clynes R. Cell surface recycling of internalized antigen permits dendritic cell priming of B cells. Immunity. 2005; 23:503–514. [PubMed: 16286018]
40. Bousso P, Robey E. Dynamics of CD8+ T cell priming by dendritic cells in intact lymph nodes. Nat Immunol. 2003; 4:579–585. [PubMed: 12730692]
41. Qi H, Egen JG, Huang AY, Germain R. Extrafollicular activation of lymph node B cells by antigen-bearing dendritic cells. Science. 2006; 312:1672–1676. [PubMed: 16778060]
42. Crocker PR, Paulson JC, Varki A. Siglecs and their roles in the immune system. Nat Rev Immunol. 2007; 7:255–266. [PubMed: 17380156]
43. Hermans IF, et al. NKT cells enhance CD4+ and CD8+ T cell responses to soluble antigen in vivo through direct interaction with dendritic cells. J Immunol. 2003; 171:5140–5147. [PubMed: 14607913]
44. De Santo C, et al. Invariant NKT cells reduce the immunosuppressive activity of influenza A virus-induced myeloid-derived suppressor cells in mice and humans. J Clin Invest. 2008; 118:4036–4048. [PubMed: 19033672]
45. Galli G, et al. Invariant NKT cells sustain specific B cell responses and memory. Proc Natl Acad Sci USA. 2007; 104:3984–3989. [PubMed: 17360464]
46. Leadbetter, et al. NK T cells provide lipid antigen-specific cognate help for B cells. Proc Natl Acad Sci USA. 2008
47. Okada T, et al. Antigen-engaged B cells undergo chemotaxis toward the T zone and form motile conjugates with helper T cells. PLoS Biol. 2005; 3:e150. [PubMed: 15857154]
48. Van Rooijen N, Sanders A. Liposome mediated depletion of macrophages: mechanism of action, preparation of liposomes and applications. J Immunol Methods. 1994; 174:83–93. [PubMed: 8083541]
49. Veerapen N, et al. Synthesis and biological activity of alpha-galactosyl ceramide KRN7000 and galactosyl (alpha1-->2) galactosyl ceramide. Bioorg Med Chem Lett. 2009; 19:4288–4291. [PubMed: 19502056]
50. Karadimitris A, et al. Human CD1d-glycolipid tetramers generated by in vitro oxidative refolding chromatography. Proc Natl Acad Sci USA. 2001; 98:3294–3298. [PubMed: 11248072]

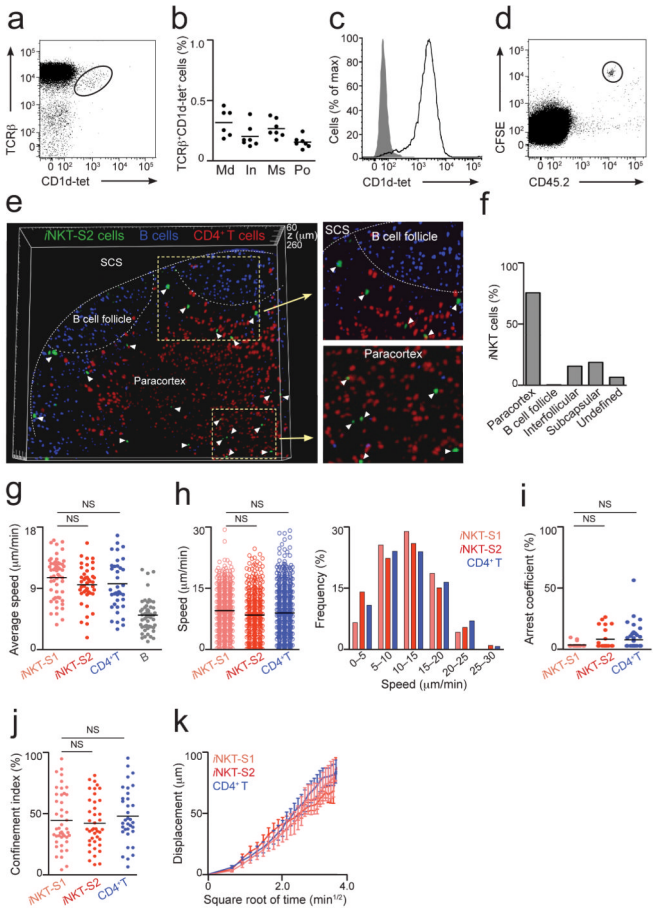

Figure 1.

Distribution and dynamics of *i*NKT cells in LNs. **(a)** *i*NKT cells in mediastinal LNs from WT animals were identified by flow cytometry as TCRβ$^+$CD1d-tet$^+$ cells. **(b)** Percentage of *i*NKT from TCRβ$^+$B220$^-$ cells in various LNs. Data is from two independent experiments with 3-4 animals per group. Md, mediastinal; In, inguinal; Ms, mesenteric; Po, popliteal. **(c)** CD1d-tet staining of *i*NKT-S2 cells. **(d)** *i*NKT-S2 cells were labelled with CFSE, transferred into CD45.1 congenic mice and detected in LNs of recipient animals as CFSE$^+$CD45.2$^+$B220$^-$. **(e,f)** *i*NKT-S2 (green), CD4$^+$ T (red) and B cells (blue) were adoptively transferred into WT recipients. LNs were fixed and imaged by multi-photon microscopy. **(e)** Three-dimensional reconstruction from a 200 μm section of a popliteal LN showing the distribution of *i*NKT cells (white arrowheads). **(f)** Percentage of *i*NKT cells in various locations in the LN. **(g-k)** *i*NKT-S1 (pale red) and *i*NKT-S2 (red) cells were adoptively transferred alongside CD4$^+$ T (blue) and/or B cells (grey). Intact LNs were imaged by multi-photon microscopy. Average speed **(g),** instantaneous speed distribution **(h)**, arrest coefficient **(i)** and confinement index **(j)** for individual cells are shown with mean values as black lines. Data were obtained in at least two independent experiments and were compared with two-tailed unpaired Mann-Whitney test. (NS, not significant) **(k)** Displacement (mean ± s.e.m) of *i*NKT and CD4$^+$ T cells plotted against the square root of time. Mean motility coefficient (*M*) can be calculated as $M=x^2/6t$, where x is the slope of the linear part of the graph.

(g-i) Each symbol represents an individual cell.

Europe PMC Funders Author Manuscripts

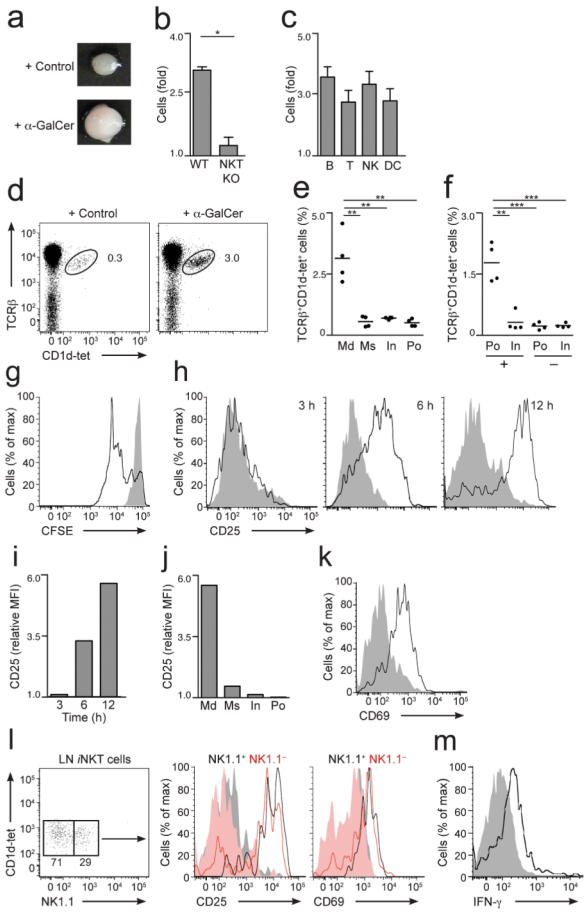

Figure 2.

Early activation of LN *i*NKT cells**. (a-f)** Animals were injected with α-GalCer or control particles and 3 days later LNs were analyzed. (**a**) Images of popliteal LNs from WT animals injected with control (top) or α-GalCer (bottom) particles. (**b**) Fold increase in total cell number (**b**) or in the depicted populations (**c**) in LNs of WT (**b,c**) and $J_{\alpha}18$ (NKT KO, **b**) mice after injection with α-GalCer particles relative to animals injected with control particles; *p<0.05 **(d)** *i*NKT cells in mediastinal LNs after i.p. injection of control (left) or α-GalCer (right) particles **(e,f)** Percentage of *i*NKT cells in various LNs after i.p. **(e)** or s.c. foot-pad **(f)** injection of α-GalCer particles. +,draining; −,non-draining LNs. Each dot represents one LN, black lines represent mean. Data were compared with two-tailed *t*-test. (p**<0.005; ***p=0.0007). **(g)** CFSE-labelled adoptively transferred *i*NKT cells were detected as $CFSE^{+}CD1d\text{-}tet^{+}TCR\beta^{+}B220^{-}DAPI^{-}$ two days after injection of α-GalCer (black) or control (grey) particles. **(h-k)** *i*NKT cell activation was measured as expression of CD25 (**h-j**) and CD69 (**k**) after i.p. injection of α-GalCer (black) or control particles (grey). MFI were normalized to mice injected with control particles. **(l)** NK1.1 expression in LN *i*NKT cells (left). Expression of CD25 (middle) and CD69 (right) in $NK1.1^{+}$ (black) and $NK1.1^{-}$ (red) *i*NKT cells in mediastinal LNs 12 h after injection with α-GalCer (empty profiles) or control particles (filled profiles). (**m**) Intracellular IFN-γ staining for mediastinal LN-*i*NKT cells 12 h after injection of α-GalCer (black) or control (grey) particles.

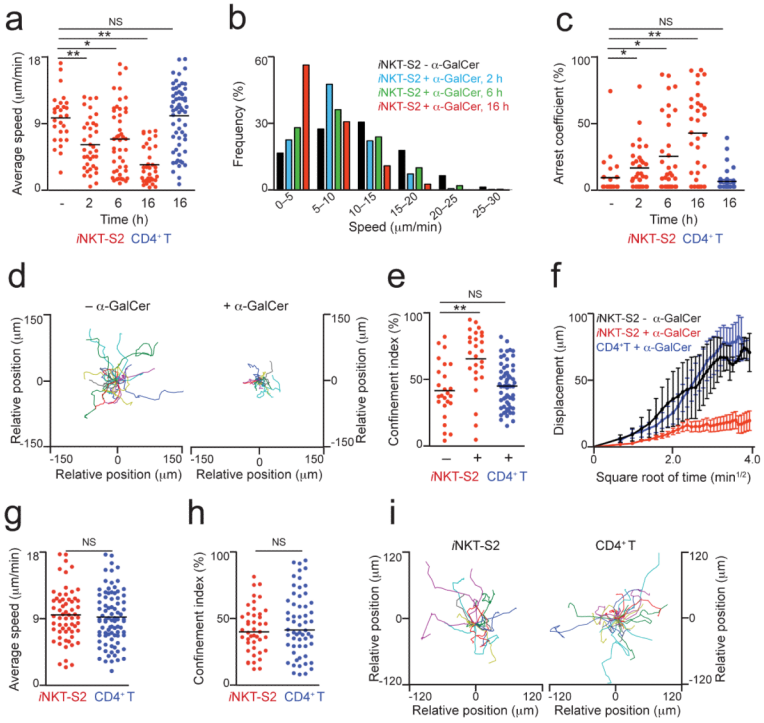

Figure 3.

*i*NKT cells arrest in the LNs in response to specific antigen. **(a-i)** *i*NKT-S2 cells (red), alongside CD4$^+$ T cells (blue), were labelled and injected i.v. into recipient mice and allowed to home for 14-16 h. **(a-f)** WT recipient mice were injected i.p. with particles coated with α-GalCer (+ α-GalCer) or control lipids (− α-GalCer) and at various time points draining mediastinal LNs were removed and imaged by multi-photon microscopy. The average speed **(a)**, instantaneous speed distribution **(b)** and arrest coefficient **(c)** of *i*NKT cells are shown at different time-points. **(d,e)** Representative migratory tracks (**d**) and confinement index **(e)** for *i*NKT cells at 16 h after injection of particulate lipids are shown. **(f)** Displacement (mean ± s.e.m.) of *i*NKT cells from mice injected with particles coated with α-GalCer (red) or control lipids (black) is plotted against the square root of time. Dynamic parameters for CD4$^+$ T cells (blue, **a,c,e,f**) at 16 h after injection of particulate α-GalCer are shown. **(g-i)** CD1d-KO recipient mice were i.p. injected with particles coated with α-GalCer and mediastinal LNs were imaged at 16 h after antigen administration. The average speed **(g)**, confinement index **(h)** and representative migratory tracks **(i)** of *i*NKT and CD4$^+$ T cells are shown. Mean values are shown as black lines. Data were obtained from at least two independent experiments per condition and were compared with a two-tailed unpaired Mann-Whitney test. *p<0.01; **p<0.0005 NS, not significant.
In a,c,e,g,h, each symbol represents one cell

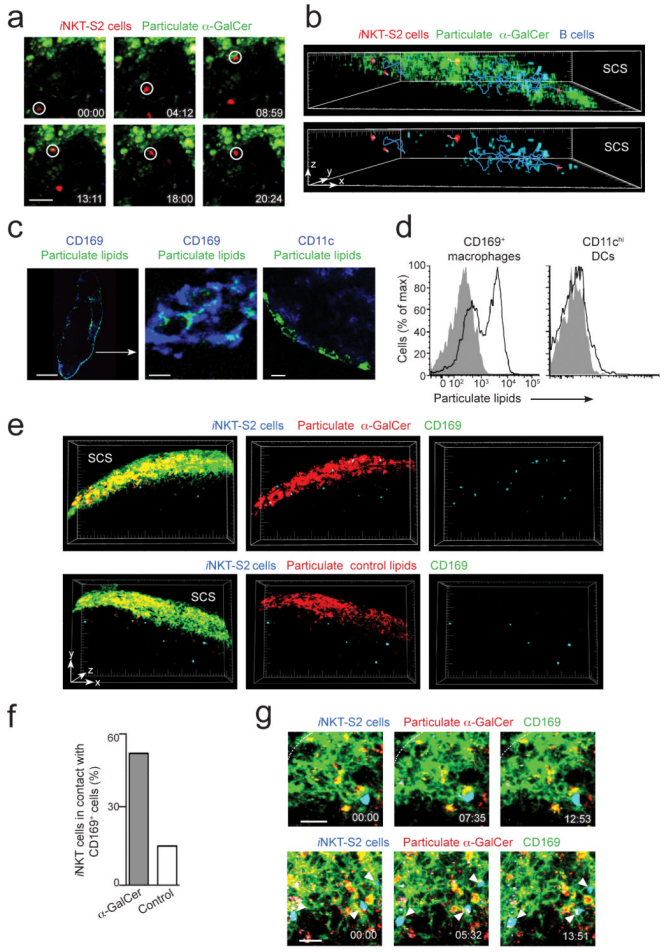

Figure 4.

*i*NKT cells arrest on SCS CD169^{+} macrophages **(a,b)** *i*NKT-S2 (red) and B cells (blue), were transferred into WT recipients prior to i.p. injection of α-GalCer particles (green). Mediastinal LNs were imaged by multi-photon microscopy. **(a)** Time-lapse images from a movie acquired 15-65 μm below the LN surface showing an *i*NKT cell arrested in the SCS (white circle) 2 h after injection of particulate α-GalCer. Scale bar, 20 μm **(b)** Three-dimensional reconstruction of the SCS 16 h after injection of particulate α-GalCer, including tracks of B and *i*NKT cells (20 min movie). **(c)** Confocal microscopy images of mediastinal LNs 2 h after i.p. injection of α-GalCer particles (green), stained with CD169 (blue, left and middle) or CD11c (blue, right). Scale bar, 300 μm (left), 5 μm (middle), 15 μm (right) **(d)** Flow cytometry analyses of lipid uptake by CD169^{+} macrophages (left) or CD11c^{hi} DCs (right) in mediastinal LNs 4 h after injection of α-GalCer particles (black). Grey, no injected **(e)** Three-dimensional reconstruction of a LN (100 μm section) after injection of α-GalCer (top) or control (bottom) particles, showing *i*NKT cells (blue), particulate lipids (red) and CD169 cells (green). Long ticks, 50 μm. **(f)** Percentage of *i*NKT cells in direct contact with CD169^{+} macrophages after injection of α-GalCer or control particles. **(g)** Time-lapse images from two different movies (top and bottom) showing *i*NKT cells (arrowheads) in contact with CD169^{+} macrophages (green) 6 h after α-GalCer (red) injection. Time stamp is in mm:ss. Scale bar, 20 μm (top), 15 μm (bottom).
Data are representative of three (a-d) or six (e-g) experiments.

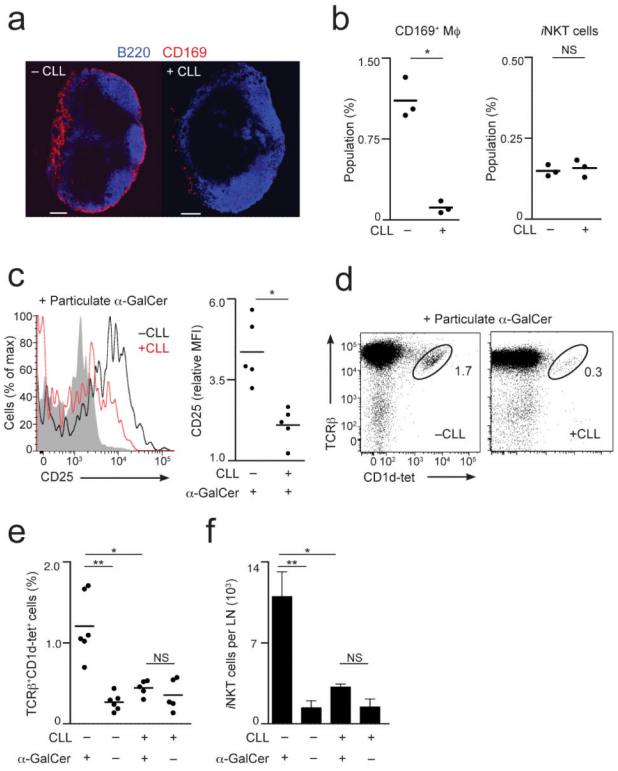

Figure 5.

Macrophages are required for early *i*NKT cell activation in the LNs **(a-f)** WT mice were injected with CLL (+CLL) or not (−CLL) 6 days prior to removal and analysis of draining LNs. **(a)** Confocal microscopy images of LNs from CCL treated (rigth) and untreated (left) mice stained for B220 (blue) and CD169 (red). **(b)** Percentage of $CD169^+$ macrophages (left) and *i*NKT cells (right) from total mononuclear cells in LNs of CLL treated or untreated mice. **p*<0.0001 **(c-f)** *i*NKT cell activation was assessed by flow cytometry after injection with α-GalCer (linear profiles) or control (grey filled profile) particles. MFI were normalized to mice injected with control particles. **(c)** CD25 expression in LN *i*NKT cells was assessed 12 h after injection of α-GalCer particles into CLL treated (red) or untreated (black) mice. **p*=0.0023 **(d-f)** Frequency of *i*NKT cells in draining LNs was assessed 3 days after injection of particles into CLL treated or untreated mice. Representative FACS profiles **(d)** and quantification of *i*NKT cell frequency **(e,** **p*=0.0025, ***p*=0.0002**)** and numbers **(f,** ***p*=0.0015; **p*=0.0408) are shown. Each data point represents one LN from individual mice. Black lines represent mean values. Data were pooled from two independent experiments and compared with a two-tailed *t*-test. NS, not significant.
Error bars (f), s.e.m.

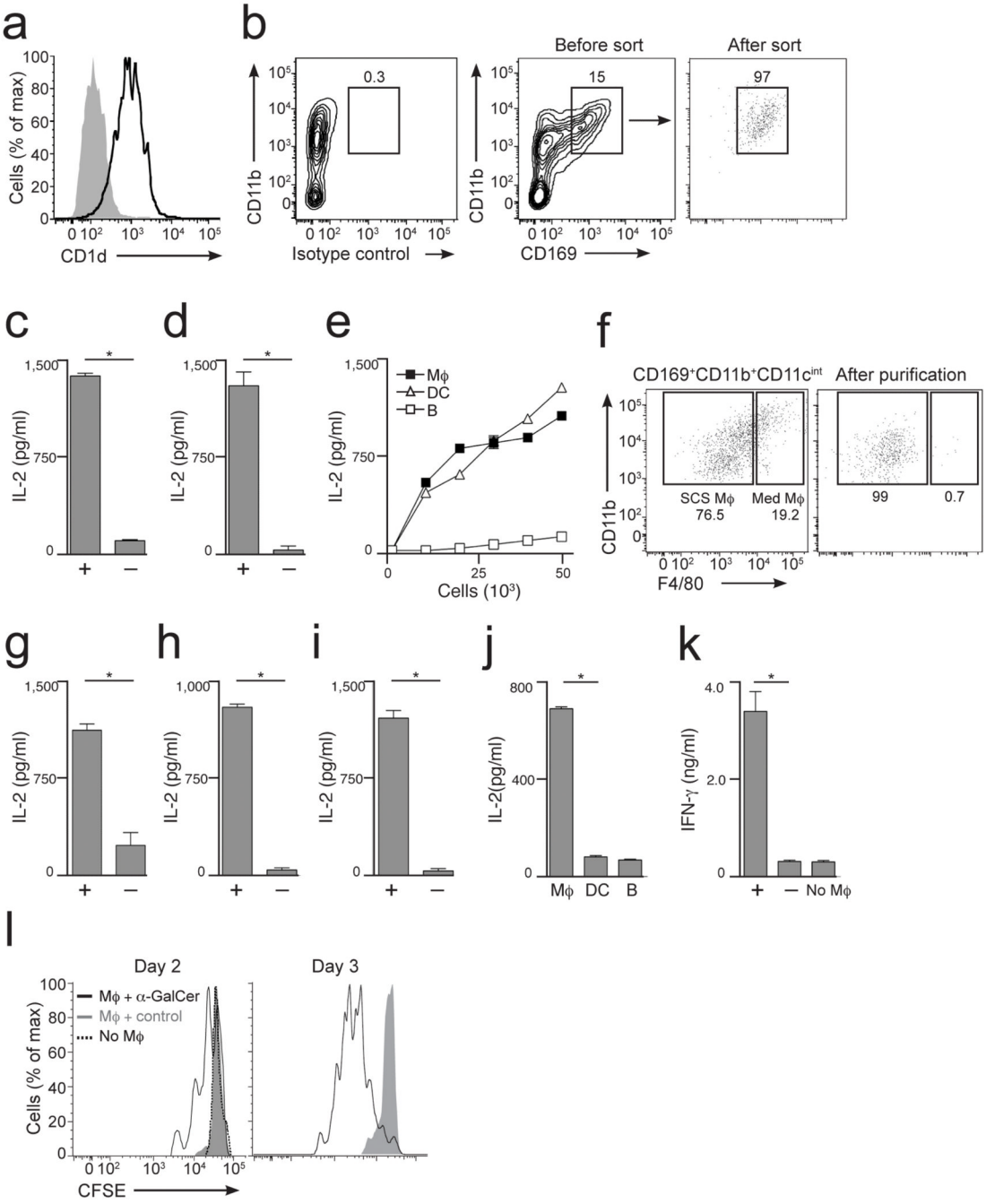

Figure 6.

LN CD169$^+$ macrophages present lipids to *i*NKT cells. **(a)** CD1d expression in CD169$^+$-CD11b$^+$ macrophages (black). Grey, isotype control. **(b)** CD11b$^+$ cells before (left, middle) or after (right) sort stained with anti-CD169 antibody (middle, right) or isotype control (left). **(c-d)** Purified CD169$^+$ cells from **b** were incubated with α-GalCer (+,**c**), Gal(α1→2)α-GalCer (+,**d**) or control (−) particles before co-culture with DN32.D3 cells. IL-2 was the read-out for lipid presentation by CD169$^+$ cells. (**e**) LN CD169$^+$ macrophages (Mφ filled squares), CD11c^{hi} DCs (triangles) and B cells (empty squares) were incubated with α-GalCer particles before co-culture (1-5 × 10^4) with 5 × 10^4 DN32.D3 cells. (**f**)

Europe PMC Funders Author Manuscripts

$CD169^+CD11b^+CD11c^{int}$ cells were stained with anti-CD11b and F4/80 antibodies before (left) and after (right) purification of SCS macrophages. (**g**) SCS macrophages were incubated with α-GalCer (+) or control (−) particles before co-culture with DN32.D3 cells **(h,i)** Mice were injected with α-GalCer (+,**h**), Gal(α1→2)α-GalCer (+,**i**) or control (−) particles and 2 h later $CD169^+$ cells from draining LNs were purified and co-cultured with DN32.D3 cells. (**j**) Mice were injected with α-GalCer particles and $CD169^+$ macrophages (Mφ), $CD11c^{hi}$ DCs and B cells were purified and co-cultured with DN32.D3 cells. (**k-l**) $CD169^+$ cells were pulsed with α-GalCer (+) or control (−) particles before co-culture (2 or 3 days) with CFSE labelled-primary *i*NKT cells purified from LNs. *i*NKT cells cultured without macrophages (No Mφ) were included as control. (**k**) IFN-γ was measured as a read-out for lipid presentation. (**l**) *i*NKT cell proliferation was detected as CFSE dilution. Data represent one experiment from at least two performed independently. Statistical analyses, two-tailed *t*-test. **p*<0.0001.
Error bars (c,d,g-k), s.e.m.

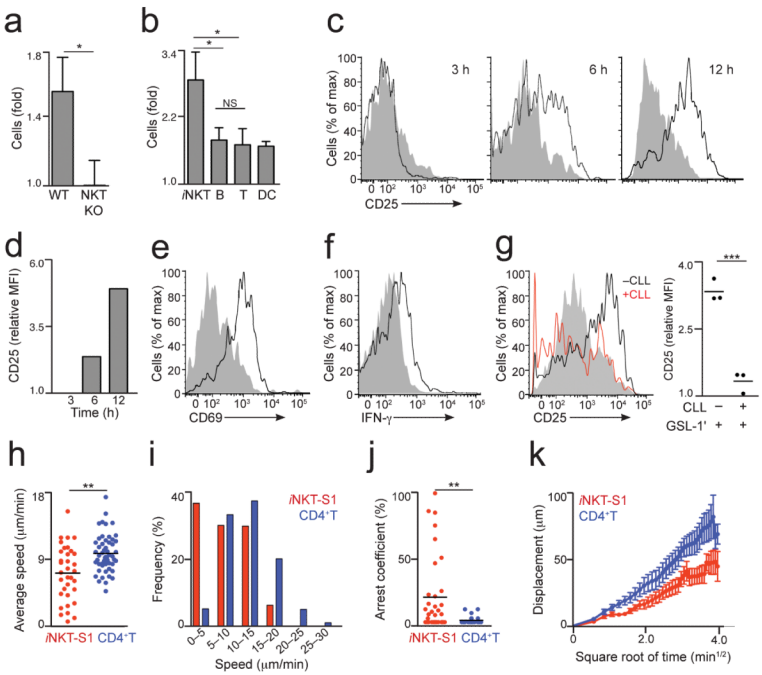

Figure 7.

Bacterial glycolipids stimulate macrophage-dependent *i*NKT cell activation (**a-b)** Fold increase in total cell number (**a**) or in the depicted populations (**b**) in LNs of WT (**a,b**) and $J_{\alpha}18$ (NKT KO, **a**) mice after injection with GSL-1′ particles relative to animals injected with control particles, **p*<0.05; NS, no significant **(c-f)** *i*NKT cell activation was assessed by flow cytometry after i.p. injection of GSL-1′ (black) or control particles (grey). **(c,d)** CD25 expression in mediastinal LN *i*NKT cells at various times after injection. MFI were normalized to mice injected with control particles. **(e,f)** Expression of CD69 **(e)** and intracellular IFN-**γ (f)** in *i*NKT cells from mediastinal LNs 12 h after injection. Data are representative of 3 independent experiments. **(g)** CD25 expression in LN *i*NKT cells was assessed 12 h after injection of GSL-1′ particles into CLL treated (red) or untreated (black) mice. MFI were normalized to mice injected with particles containing control lipids. Black lines indicate mean values. Data points represent one mediastinal LN from individual mice and representative from two independent experiments with at least 2 animals per experiment. Data were compared with two-tailed *t*-test, ****p*=0.0006. (**h-k**) *i*NKT-S1 (red) and $CD4^{+}$T cells (blue) were transferred into WT recipients injected i.p. with GSL-1′ particles. Average speed **(h)**, instantaneous speed distribution **(i),** arrest coefficient **(j)** and mean displacement (± s.e.m., **k**) for *i*NKT and $CD4^{+}$T cells are shown at 16 h after antigen administration. Data were obtained from at least two independent experiments and compared with a two-tailed unpaired Mann-Whitney test. ***p*<0.005

Error bars (a,b), s.e.m.

Europe PMC Funders Author Manuscripts